Chinese Chemical Letters 35 (2024) 109181

Contents lists available at ScienceDirect

Chinese Chemical Letters

journal homepage: www.elsevier.com/locate/cclet

Core–shell heterostructure engineering of CoP nanowires coupled NiFe LDH nanosheets for highly efficient water/seawater oxidation

Guo-Hong Gao[a,1], Run-Ze Zhao[b,1], Ya-Jun Wang[a], Xiao Ma[a], Yan Li[a], Jian Zhang[a,*], Ji-Sen Li[a,c,*]

[a] School of Chemistry, Chemical Engineering and Materials, Jining University, Qufu 273155, China
[b] Institute of Physical Education, Jining University, Qufu 273155, China
[c] Key Laboratory of Advanced Energy Materials Chemistry (Ministry of Education), Nankai University, Tianjin 300071, China

ARTICLE INFO

Article history:
Received 30 August 2023
Revised 17 September 2023
Accepted 6 October 2023
Available online 11 October 2023

Keywords:
Cobalt phosphide
NiFe layered double hydroxide
Interfacial engineering
Oxygen evolution reaction
Seawater oxidation

ABSTRACT

Searching for efficient nonprecious metal-based catalysts toward oxygen evolution reaction (OER) are of significance for seawater electrolysis. Herein, a core–shell-structured hybrid of cobalt phosphide nanowires@NiFe layered double hydroxide nanosheets grown on conductive nickel foam (CoP@NiFe LDH/NF) is prepared by a feasible approach at low temperature. The charming structure can provide numerous phosphide/hydroxide heterogenous interfaces, expose abundant active sites, and boost electron/mass transfer, synergistically enhancing catalytic OER activity. When employed as an electrocatalyst toward the OER, the resultant CoP@NiFe LDH/NF only requires a small overpotential of 287 mV to provide 300 mA/cm^2 current density as well as long-time durability in 1.0 mol/L KOH seawater. The regulation of electronic states and surface reconstruction synergistically contribute to highly efficient seawater oxidation. This work provides an opportunity to construct efficient and inexpensive electrocatalysts for hydrogen production.

Hydrogen (H_2) with high purity is expected to be a promising replacement to fossil fuel. Among numerous approaches, electrochemical water splitting by storing sustainable energies such as solar, wind, and biomass is a potential technology for industrial H_2 generation [1,2]. In comparison with the cathodic hydrogen evolution reaction, the anodic oxygen evolution reaction (OER) encounters more sluggish kinetics, greatly restricting the efficiency of water splitting [3–6]. At present, RuO_2 and IrO_2 as benchmark catalysts toward OER are almost important to be widely performed because of their high cost and scarcity [7–10]. To overcome the dilemma, the development of efficient cheap electrode materials such as phosphides [11–14], transition-metal (hydro) oxides [15–20], sulfides [21–23] for OER has attracted extensive attentions. At present, most of these electrocatalysts reported operate well in freshwater feeds. However, larger quantities of highly pure water feeds are deemed a bottleneck, especially for coastal, hyper-arid regions and islands [24,25]. As is well-known, seawater representing 96.5% of the global water reserve, is an almost inexhaustible resource for water splitting. The fatal obstacle for seawater electrolysis under alkaline media originates from the chlorine oxidation reaction, which would compete with the OER [26–28]. Besides, insoluble precipitations or microbes will lead to poisoning the electrode materials and weakening their electrocatalytic activity and stability [29].

On the basis of these factors, it is of grand urgency to exploit advanced inexpensive catalysts toward seawater electrolysis. In this regard, electrode materials with outstanding catalytic OER performance under natural seawater conditions should possess many fascinating advantages including impressive intrinsic electroactivity, large active surface area, porous structure, plentiful accessible active centers, high conductivity, and chloride-corrosion resistance [30–32]. Noteworthily, NiFe layered double hydroxides (NiFe LDH) rank among the most competitive alternatives due to the tunable component and structure merits [33–37]. Regrettably, their lower active sites and inherent nonconductivity severely hamper the large-scale applications for OER [38,39]. To this end, multitudinous methods have been employed to boost the electrocatalytic activity of NiFe LDH hybrid toward seawater oxidation [40–45]. Despite great progress, there is a great deal of room for exploitation of highly efficient OER electrocatalysts with excellent corrosion resistance under natural seawater media.

* Corresponding authors.
E-mail addresses: sduchemzhang@163.com (J. Zhang), senjili@sina.com (J.-S. Li).
[1] These authors contributed equally to this work.

https://doi.org/10.1016/j.cclet.2023.109181
1001-8417/

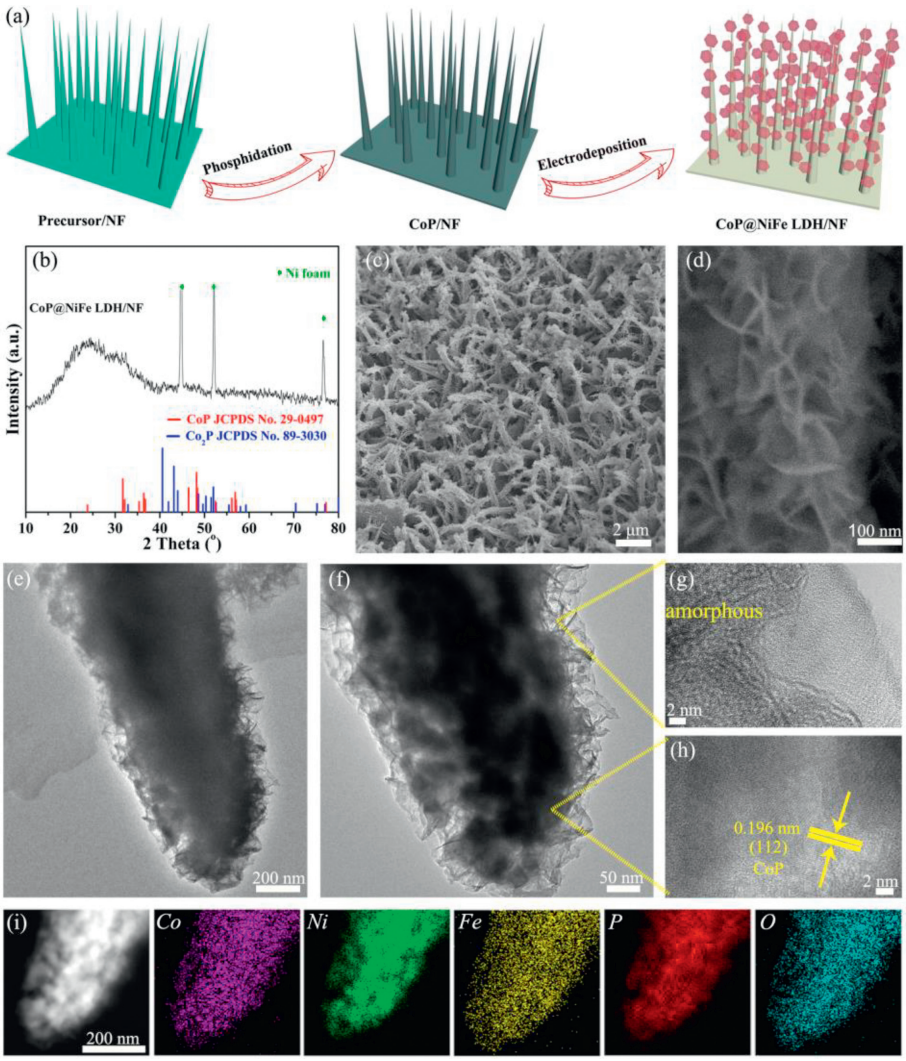

Fig. 1. (a) Schematic illustration of the preparation of CoP@NiFe LDH/NF. (b) PXRD pattern, (c and d) SEM, (e, f) TEM, (g, h) high-resolution TEM, and (i) EDS element mapping images of CoP@NiFe LDH/NF.

Encouraged by the above-mentioned, we propose a feasible interface engineering strategy to synthesize heterostructured cobalt phosphide nanowires@NiFe LDH sheets on nickel foam (CoP@NiFe LDH/NF). The attractive architecture is not only conducive to increase of specific surface area and exposure of accessible catalytic centers, but favorable to close contact of CoP nanowires and NF substrate and improvement of electron/mass transfer. Additionally, the interfacial effect between CoP nanowires and NiFe LDH nanosheets can powerfully modulate the electronic states of active species, further improving electrocatalytic efficiency. Benefitting from the above, the CoP@NiFe LDH/NF only requires the low overpotentials of 265 and 277 mV to provide 300 mA/cm^2 current density in alkaline and simulated seawater media, respectively. Particularly, the CoP@NiFe LDH/NF can work well and continuously operate for 10 h in alkaline natural seawater.

As depicted in Fig. 1a, the core–shell heterostructure of CoP@NiFe LDH/NF was fabricated through a facile multistep hydrothermal-phosphidation-electrodeposition approach. Herein, NF was chosen as binder-free conductive support with effective mechanical strength. First, precursor nanowires were arrayed on NF (precursor/NF) by a hydrothermal reaction according to previous literature [13]. In Fig. S1 (Supporting information), the powder X-ray diffraction pattern (PXRD) shows the precursor consists of Co(OH)F and $Co(CO_3)_{0.5}(OH)$. The other three typical diffraction peaks correspond to NF substrates. As seen from scanning electron microscopy (SEM) images (Fig. S2 in Supporting information), the precursor nanowire arrays vertically decorated on NF. Then, the resultant precursor/NF was transformed into CoP/NF *via* a simple phosphidation process, which can be confirmed by the corresponding PXRD pattern in Fig. S3 (Supporting information). Although the resultant CoP/NF hybrid well retains the nanowire arrays shape (Fig. S4 in Supporting information), the surface of nanowire becomes rough compared to the precursor, stemming from dehydration and gas release [13]. Lastly, the CoP nanowires core was fully covered by NiFe LDH nanosheets shell with an electrodeposition strategy (CoP@NiFe LDH/NF). Unexpectedly, no new diffraction peak is appeared except for the typical peaks from CoP and NF (Fig. 1b), which strongly verifies that NiFe LDH nanosheets are amorphous in nature [37]. The SEM images of the resulting CoP@NiFe LDH/NF exhibit that untrathin NiFe LDH nanosheets are arranged on CoP nanowires (Figs. 1c and d), implying the production of CoP/NiFe LDH heterostructure. Additionally, NiFe LDH/NF hybrid was also constructed through an identical method for comparison (Fig. S5 in Supporting information). Transmission electron microscope (TEM) was applied to examine the structure characteristic in detail (Figs. 1e and f). It is found that the NiFe LDH nanosheets shells are decorated on the surface of the CoP nanowires cores, implying the formation of heterostructure. Interestingly, these NiFe

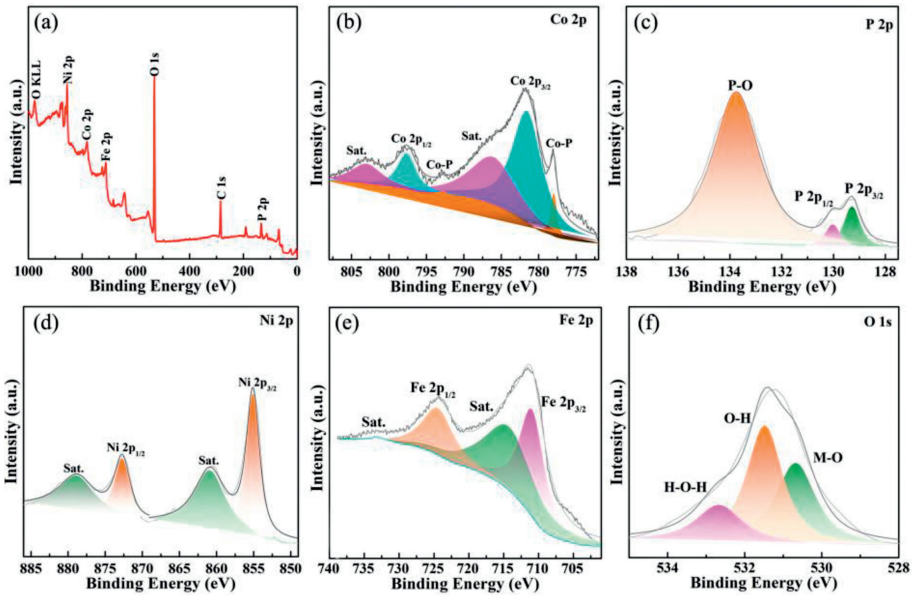

Fig. 2. (a) XPS survey spectrum, high-resolution XPS of Co 2p (b), P 2p (c), Ni 2p (d), Fe 2p (e), and O 1s (f) for CoP@NiFe LDH/NF, respectively.

LDH nanosheets are interconnected with each other, leading to rich pores and exposed active sites. Likewise, the conductive CoP nanowires are favorable to accelerate electron transfer. In addition, the NiFe LDH shell presents the amorphous feature (Fig. 1g), while the lattice spacing of 0.196 nm belonging to (112) plane of orthorhombic CoP can be obviously observed (Fig. 1h) [14]. In Fig. 1i, the heterostructure of CoP@NiFe LDH is manifested by the EDS element mapping images. Consequently, the above data significantly elucidate that a CoP@NiFe LDH heterostructure catalyst was successfully constructed through a feasible strategy.

The electronic structure and valence of targeted catalysts were investigated by X-ray photoelectron spectroscopy (XPS). Fig. 2a reveals that the CoP@NiFe LDH/NF consists of Co, P, Ni, Fe, and O elements. In Fig. 2b, the Co 2p spectrum is deconvoluted into three doublets at 777.9/792.8, 781.5/797.6, and 786.1/802.9 eV, indicative of Co–P, Co oxides, and satellite peaks (Sat.), respectively [14]. Furthermore, it is found that the Co 2p peaks of CoP@NiFe LDH/NF are shifted negatively compared to that of the CoP/NF (Fig. S6 in Supporting information) [14]. In terms of the P 2p spectrum (Fig. 2c), the binding energies at 129.3 and 130.1 eV can be ascribed to P–Co bond. The additional binding energy at 133.8 eV can be clearly seen due to surface oxidation [13,31]. The Ni 2p XPS spectrum in Fig. 2d depicts that the peaks of 855.1 and 872.7 eV are attributed to Ni^{3+} $2p_{3/2}$ and Ni^{3+} $2p_{1/2}$ originating from NiFe LDH [19], which present a positive shift relative to that of NiFe LDH/NF (Fig. S6). The other peaks of 860.8 and 878.9 eV belong to shake-up satellites. As for the Fe 2p XPS spectrum in Fig. 2e, two fitting peaks at 710.9 and 724.4 eV correspond to Fe^{3+} $2p_{3/2}$ and Fe^{3+} $2p_{1//2}$ along with two satellites at 714.2 and 733.0 eV [42]. In Fig. 2f, the peaks at 530.7, 531.5, and 532.7 eV are assigned to M-O, O–H, and H–O-H, respectively [21]. Considering the aforementioned results, the formation of CoP/NiFe LDH heterostructure can modulate the surface electronic structure, thereby effectively promoting catalytic OER performance.

The electrocatalytic OER performance of targeted catalysts was assessed with a standard three-electrode apparatus in 1.0 mol/L KOH. In Fig. 3a, linear sweep voltammetry (LSV) polarization curves with 95% iR-corrected exhibit that the electrocatalytic behavior follows the trend of CoP@NiFe LDH/NF > NiFe LDH/NF > CoP/NF > IrO_2/NF. It is worth pointing out that the existence of heterointerface between NiFe LDH sheets shells and CoP nanowires core has a crucial effect on enhancing the electrocatalytic OER performance. Impressively, the as-prepared CoP@NiFe LDH/NF merely needs the overpotentials of only 203, 226 and 238 mV to deliver 10, 50 and 100 mA/cm^2, respectively, lower than that of NiFe LDH/NF (236, 266 and 287 mV), CoP/NF (246, 294 and 313 mV), and IrO_2/NF (321, 445 and 499 mV), displayed in Fig. 3b. To optimize the electrodeposition time, the CoP@NiFe LDH/NF catalysts were pre-synthesized with different electrodeposition time (60, 90, and 120 s). As indicated in Fig. S7 (Supporting information), the CoP@NiFe LDH/NF with 90 s electrodeposition treatment possesses the best catalytic performance, signifying that the appropriate ratio of LDH phase in the heterojunction plays a substantial role in the catalytic OER activity in 1.0 mol/L KOH. In Fig. 3c, the Tafel slope of 35.4 mV/dec for the targeted CoP@NiFe LDH/NF is considerably smaller than that of NiFe LDH/NF (44.7 mV/dec), CoP/NF (64.5 mV/dec), and IrO_2/NF (88.1 mV/dec). The lower value implies a rapid kinetics for electrochemical water oxidation originating from the component and core-shell heterostructure. Impressively, the catalytic OER behavior of CoP@NiFe LDH/NF can compare to that of many advanced electrocatalysts previously reported (Table S1 in Supporting information) [14,22,23]. Besides, the electrochemically active surface areas (ECSA) of the three catalysts were assessed by the corresponding double-layer capacitance (C_{dl}), which was achieved by cyclic voltammetry (CV) scans (Fig. S8 in Supporting information). As revealed in Fig. 3d, the C_{dl} value of the resulting CoP@NiFe LDH/NF is calculated to be ~10.5 mF/cm^2, 5.2 and 1.5 times that of NiFe LDH/NF (2.0 mF/cm^2) and CoP/NF (7.1 mF/cm^2). This result means that numerous accessible active sites are exposed on the surface of CoP@NiFe LDH/NF, resulting in improved catalytic OER performance. Furthermore, the CoP@NiFe LDH/NF still presents the primary electroactivity after being normalized by ECSA (Fig. S9 in Supporting information), confirming its higher intrinsic catalytic OER behavior [23]. As is well known, long-time stability is also a pivotal parameter to evaluate the practical application of targeted catalysts. The multi-step chronopotentiometric curve of CoP@NiFe LDH/NF in Fig. 3e demonstrates that the applied potential is almost unchanged within the applied current densities, and the same voltage can be achieved throughout the reverse process, suggesting the fast mass transport and robust architecture of CoP@NiFe LDH/NF. In Fig. 3f, the LSV plot after 1000 mostly coincides with the initial plot. Furthermore, the CoP@NiFe

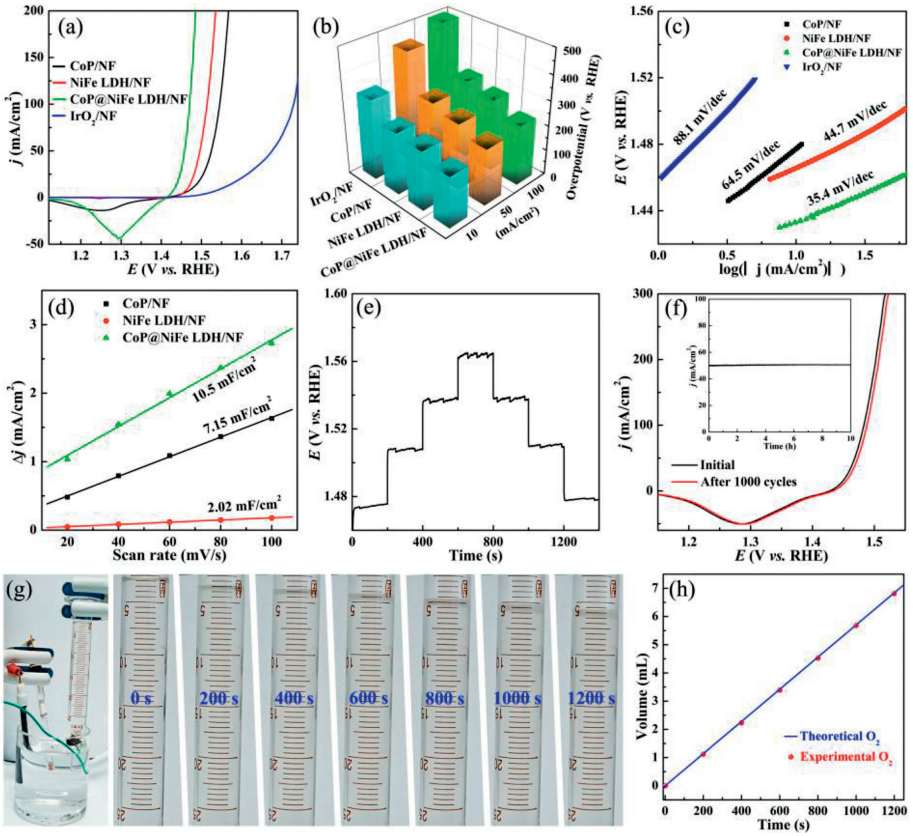

Fig. 3. (a) OER polarization plots, (b) comparisons of overpotential at 10, 50 and 100 mA/cm^2, (c) Tafel slopes, (d) double-layer capacitance (C_{dl}) of different catalysts. (e) Multi-steps chronopotentiometry curves of CoP@NiFe LDH/NF, (f) LSV curves of CoP@NiFe LDH/NF after 1000 cycles. Inset of (d) chronoamperometric curve of CoP@NiFe LDH/NF at 50 mA/cm^2. (g) Gas collection device for OER and digital photographs of O_2 generated at different time. (h) Gas volume of produced O_2 *versus* time.

LDH/NF maintains stable catalytic OER performance for 10 h (inset of Fig. 3f). Accordingly, the afore-mentioned results strongly evidence the outstanding durability of CoP@NiFe LDH/NF in alkaline media. Additionally, a water drainage approach was employed to collect the amount of O_2 generated by CoP@NiFe LDH/NF (Fig. 3g). As exhibited in Fig. 3h, the volume ratio of theoretical and experimental O_2 is close to 2:1, indicative of nearly 100% Faradaric efficiency.

The composition and morphology of CoP@NiFe LDH/NF after durability test were examined by PXRD, SEM, and XPS, respectively. As seen from the PXRD pattern (Fig. S10a in Supporting information), the characteristic peak intensity distinctly reduces owing to surface reconstruction. The SEM image in Fig. S10b (Supporting information) exhibits the well-preserved core-shell heterostructure, which powerfully validates that the excellent long-term durability for the OER may profit from the 3D porous framework and monolithic electrode construction. The structure can facilitate the release of bubbles, expose rich accessible active sites, and expedite electron/mass transfer [31]. Surprisingly, the peaks corresponding to Co–P and P–Co nearly disappear in Figs. 4a and b, suggesting the partial leaching of P element. In parallel, the Ni 2p and Fe 2p spectra show evident positive shift in comparison to the pristine catalyst (Figs. 4c and d), reconfirming that the surface Ni and Fe ions can be oxidized to higher valence states. Accordingly, the excellent catalytic OER performance may be ascribed to the following reasons: (1) The core-shell heterostructure is favorable to the modulation of electronic structure and redistribution of electron, thereby promoting water splitting. Moreover, the charming nanostructure can expose more accessible active sites and enhance the intrinsic electroactivity of electrode materials [9]. (2) CoP nanowires@NiFe LDH nanosheets *in situ* arrayed on NF enables active sites to closely

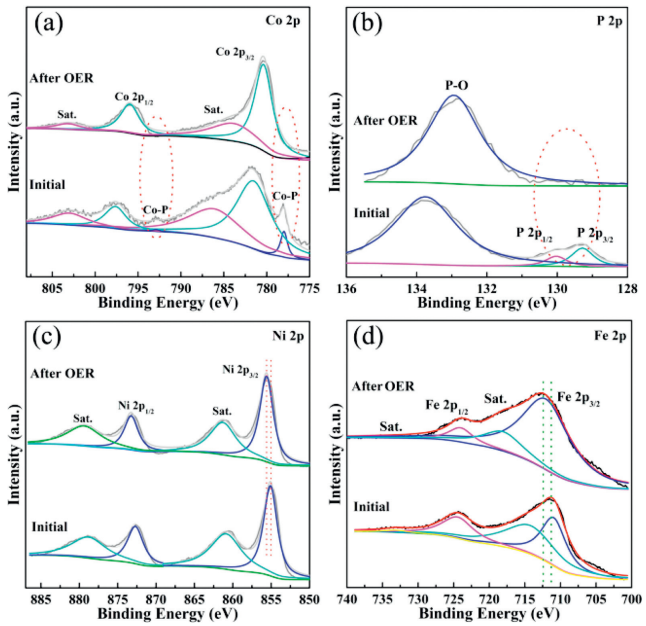

Fig. 4. High-resolution XPS spectra of (a) Co 2p, (b) P 2p, (e) Ni 2p, and (f) Fe 2p for CoP@NiFe LDH/NF after stability test, respectively.

contact with the electrolytes and accelerates gas bubbles releasing [45]. (3) The *in situ* produced Ni(Fe)OOH species during the oxidative reconstruction process are expected to be the really active components toward OER [21,37].

In view of the remarkable electrochemical OER behavior of CoP@NiFe LDH/NF in 1.0 mol/L KOH, the OER activity was fur-

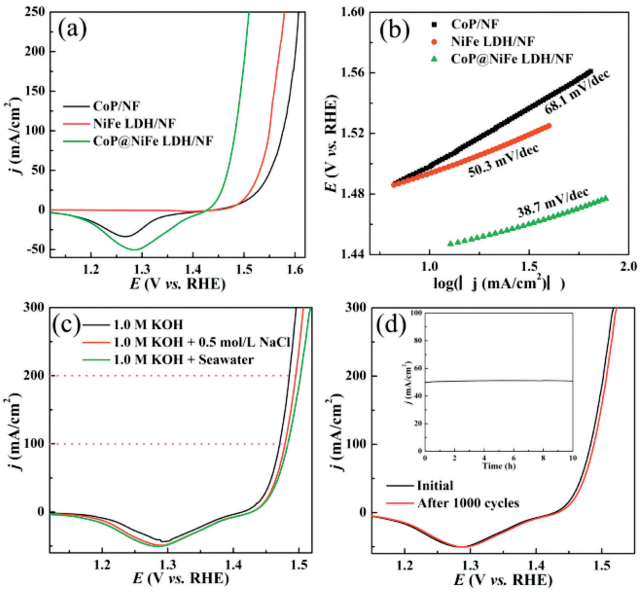

Fig. 5. (a) LSVs and (b) corresponding Tafel plots of different catalysts in natural alkaline seawater. (c) LSVs of CoP@NiFe LDH/NF under different media. (d) LSVs before and after 1000 cycles in alkaline natural seawater. Inset: chronoamperometry curve of CoP@NiFe LDH/NF.

ther assessed in simulated seawater (1.0 mol/L KOH + 0.5 mol/L NaCl) and natural alkaline seawater (1.0 mol/L KOH + seawater). As demonstrated in Fig. 5a, the resultant CoP@NiFe LDH/NF can maintain excellent electrocatalytic OER behavior in natural alkaline seawater, which merely needs overpotentials of 250 and 280 mV to offer 100 and 250 mA/cm^2 current density, respectively. In contrast, the overpotentials of 350 and 380 mV for NiFe LDH/NF and CoP/NF to obtain 250 mA/cm^2, respectively. In Fig. 5b, the measured catalysts show much lower OER kinetics in natural alkaline seawater in comparison with 1.0 mol/L KOH. The Tafel slopes of CoP@NiFe LDH/NF, NiFe LDH/NF, and CoP/NF are 38.7, 68.1, and 50.3 mV/dec, respectively, confirming that CoP@NiFe LDH/NF still has an energetic OER electrocatalytic kinetics under alkaline seawater. Moreover, the catalytic performance of CoP@NiFe LDH/NF in 1.0 mol/L KOH + 0.5 mol/L NaCl solution is inferior to that in 1.0 mol/L KOH (Fig. 5c). To provide 300 mA/cm^2, an overpotential of 277 mV is required, only 12 mV larger than that in 1.0 mol/L KOH. The electrochemical behavior of the resultant CoP@NiFe LDH/NF in natural alkaline seawater is further attenuated, and the required overpotential (287 mV) at 300 mA/cm^2 is 22 mV higher than that in 1.0 mol/L KOH. The results may be related to the presence of microbes, insoluble precipitates, and bacteria, which can block partial active centers or poison the electrode [17,21]. Additionally, the CoP@NiFe LDH/NF also exhibits excellent long-term stability for the OER in alkaline natural seawater, which can be proven by LSV after 1000 cycles and chronoamperometry measurement (Fig. 5d and Fig. S11 in Supporting information). Consequently, the CoP@NiFe LDH/NF as nonprecious metal-based electrocatalyst ranks many advanced OER electrocatalysts reported in alkaline seawater media (Table S2 in Supporting information) [14,16,21].

In summary, the heterostructured electrocatalyst of CoP@NiFe LDH/NF has been fabricated by NiFe LDH nanosheets covered on CoP nanowires. A variety of characterization measurements demonstrate the surface reconstruction and regulation of electronic states on catalytic active sites. As expected, the resultant CoP@NiFe LDH/NF shows excellent electrocatalytic OER performance as well as long-term durability, which merely needs the overpotentials of 265 and 287 mV to deliver 300 mA/cm^2 current density, respectively, in alkaline media and alkaline seawater. This finding offers new route in the fabrication of efficient inexpensive OER catalysts toward hydrogen generation by seawater electrolysis.

Declaration of competing interest

The authors declare no competing financial interests.

Acknowledgments

Financial support from the National Natural Science Foundation of China (No. 21971086) and University Feature Laboratory for Energy Conversion and Nanocatalysis of Shandong Province.

Supplementary materials

Supplementary material associated with this article can be found, in the online version, at doi:10.1016/j.cclet.2023.109181.

References

[1] J.A. Turner, Science 305 (2004) 972–974.
[2] Z. Wu, P. Yang, Q. Li, et al., Angew. Chem. Int. Ed. 62 (2023) e202300406.
[3] L. Kang, J. Li, Y. Wang, et al., J. Colloid. Interface Sci. 630 (2023) 257–265.
[4] L. Li, P. Wang, Q. Shao, X. Huang, Chem. Soc. Rev. 49 (2020) 3072–3106.
[5] J. Xu, M. Li, B. Dong, L. Feng, Chin. Chem. Lett. 35 (2024) 108798.
[6] H. Wang, P. Yang, X. Sun, et al., J. Energy Chem. 87 (2023) 286–294.
[7] Z. Zhuang, Y. Wang, C.Q. Xu, et al., Nat. Commun. 10 (2019) 4875.
[8] D. Zhang, M. Li, X. Yong, et al., Nat. Commun. 14 (2023) 2517.
[9] Y. Li, W. Wang, M. Cheng, et al., Adv. Mater. 35 (2023) 2206351.
[10] G. Chang, Y. Zhou, J. Wang, et al., Small 19 (2023) 2206768.
[11] M. Li, X. Wang, K. Liu, et al., Adv. Energy Mater. 13 (2023) 2301162.
[12] J.T. Ren, L. Chen, H.Y. Wang, et al., ACS Catal. 13 (2023) 9792–9805.
[13] X. Yu, J. Zhao, M. Johnsson, Adv. Funct. Mater. 31 (2021) 2101578.
[14] L. Wu, L. Yu, B. McElhenny, et al., Appl. Catal. B: Environ. 294 (2021) 120256.
[15] Y. Gao, D. Zheng, Q. Li, et al., Adv. Funct. Mater. 32 (2022) 2203206.
[16] D. Feng, P. Wang, R. Qin, et al., Adv. Sci. 10 (2023) 2300342.
[17] L. Chen, Y. Wang, X. Zhao, et al., J. Mater. Sci. Technology 110 (2022) 128–135.
[18] Y. Zhao, Q. Wen, D. Huang, et al., Adv. Energy Mater. 13 (2023) 2203595.
[19] P. Ding, H. Song, J. Chang, S. Lu, Nano Res. 15 (2022) 7063–7070.
[20] L. Gao, X. Zhong, J. Chen, et al., Chin. Chem. Lett. 34 (2023) 108085.
[21] J.T. Ren, L. Chen, W.W. Tian, et al., Small 19 (2023) 2300194.
[22] L. Tan, J. Yu, C. Wang, et al., Adv. Funct. Mater. 32 (2022) 2200951.
[23] X. Luo, P. Ji, P. Wang, et al., Adv. Sci. 9 (2022) 210484.
[24] S. Dresp, F. Dionigi, M. Klingenhof, P. Strasser, ACS Energy Lett. 4 (2019) 933–942.
[25] W. Tong, M. Forster, F. Dionigi, et al., Nat. Energy 5 (2020) 367–377.
[26] L. Wu, L. Yu, Q. Zhu, et al., Nano Energy 83 (2021) 105838.
[27] F. Dionigi, T. Reier, Z. Pawolek, M. Gliech, P. Strasser, ChemSusChem 9 (2016) 962–972.
[28] Z. Chen, Q. Li, H. Xiang, et al., Inorg. Chem. Front. 10 (2023) 1493–1500.
[29] X. Liu, J. Chi, H. Mao, L. Wang, Adv. Energy Mater. 13 (2023) 2301438.
[30] J.S. Ko, J.K. Johnson, P.I. Johnson, Z. Xia, ChemCatChem 12 (2020) 4526–4532.
[31] S. Yang, J.Y. Zhu, X.N. Chen, et al., Appl. Catal. B: Environ. 304 (2022) 120914.
[32] H. You, D. Wu, D. Si, et al., J. Am. Chem. Soc. 144 (2022) 9254–9263.
[33] Y. Li, H. Xu, P. Yang, et al., Mater. Today Energy 25 (2022) 100975.
[34] Y. Li, Y. Sun, Y. Qin, et al., Adv. Energy Mater. 10 (2020) 1903120.
[35] S. Dresp, F. Dionigi, M. Klingenhof, et al., ACS Catal. 11 (2021) 6800–6809.
[36] L. Zhou, C. Zhang, Y. Zhang, Z. Li, M. Shao, Adv. Funct. Mater. 31 (2021) 2009743.
[37] X. Lu, C. Zhao, Nat. Commun. 6 (2015) 6616.
[38] L. Peng, N. Yang, Y. Yang, et al., Angew. Chem. Int. Ed. 60 (2021) 24612–24619.
[39] W. Chen, B. Wu, Y. Wang, et al., Energy Environ Sci 14 (2021) 6428–6440.
[40] T. Li, X. Zhao, M. Getaye Sendeku, et al., Chem. Eng. J. 460 (2023) 141413.
[41] X. He, X. Han, X. Zhou, et al., Appl. Catal. B: Environ. 331 (2023) 122683.
[42] Y. Hu, T. Shen, Z. Song, et al., ACS Catal. 13 (2023) 11195–11203.
[43] M. Hao, Z. Xu, X. Liu, et al., Inorg. Chem. Front. 10 (2023) 1603–1613.
[44] H. Lei, Q. Wan, S. Tan, Z. Wang, W. Mai, Adv. Mater. 35 (2023) 2208209.
[45] P. Zhai, C. Wang, Y. Zhao, et al., Nat. Commun. 14 (2023) 1873.